School of Pharmacy[1], Fudan University; China State Institute of Pharmaceutical Industry[2]; Shanghai Center for Drug Evaluation and Inspection[3], Shanghai, China

Polymer selection for amorphous solid dispersion of a new drug candidate by investigation of drug polymer molecular interactions

Bin Hu[1,2,#], Zhiliang Lv[2,#], Guiliang Chen[2,3,*], Jianzhong Lu[1,*]

Received September 30, 2022, accepted August 11, 2023

**Corresponding authors: Guiliang Chen, China State Institute of Pharmaceutical Industry, 285 Gebaini Road, Shanghai 201203, China*
chenguiliang@smda.sh.cn
Jianzhong Lu, School of Pharmacy, Fudan University, 826 Zhangheng Road, Shanghai 201203, China
jzlu@shmu.edu.cn
[#]These two authors contributed equally to this work.

Pharmazie 78: 185-195 (2023) *doi: 10.1691/ph.2023.2061*

The antitumor drug candidate X-05 is being developed as an innovative anti-lung cancer drug candidate due to its excellent antitumour activity. A Caco-2 cell permeability study and solubility study confirmed that X-05 belonged to BCS class II or IV compounds. Therefore, the main challenge is to develop appropriate preparations for preclinical studies and further clinical phase research. By evaluating the preliminary results of kinetic solubility in biorelevant media and the structural analysis of X-05 and polymers, three polymers PVP K30, PVP VA 64 and HPMCAS, which may have intermolecular interactions with X-05, were chosen to select the optimal carrier for X-05 to prepare amorphous solid dispersions (ASDs). ASD X-05-PVP VA 64 was selected as the optimal polymer by evaluating its kinetic solubility in biorelevant media and solid stability. The physical and chemical properties of ASD X-05-PVP VA 64 remain stable when the drug loading is as high as 50%. The drug-polymer interactions of ASD X-05-PVP VA 64 were studied by ultraviolet spectrophotometry, nuclear magnetic resonance spectrometry, infrared and Raman spectrophotometry, and the results indicated that the intermolecular hydrogen bond interaction between the drug and polymer was the foundation of the solubilization and stabilization of X-05 in PVP VA 64.

1. Introduction

For several decades, crystal form selection has been the main goal of synthetic chemists to obtain proper crystalline forms of drug candidates for pharmaceutical development because the tight packing of molecules in the crystal lattice usually ensures a higher level of chemical purity and solid-state stability (Newman 2015). On the other hand, compounds with high crystallinity usually have lower aqueous solubility due to their high lattice energy (Niazi 2007). According to the classical Noyes-Whitney equation (Noyes and Whitney 1897), drugs with low aqueous solubility would be expected to exhibit low dissolution rates and, most likely, poor oral bioavailability (Amidon et al. 1995). With the wide application of combinatorial chemistry and high-throughput screening, the speed of discovering new chemical entities (NCEs) has dramatically increased (Cook et al. 2014). However, approximately 40% of NCEs and nearly 90% of drug candidates in the pipeline are poorly soluble molecules (Kalepu and Nekkanti 2015; Newman 2015; Tran et al. 2019), which has presented a significant challenge in the development of a suitable formulation for oral administration.

During pharmaceutical technology development, some strategies could be used to improve the aqueous solubility of drugs, such as reducing the particle size of drug substances, adding solubilizers to reduce the surface tension of drug particles in aqueous solution, using cyclodextrins to prepare inclusion complexes, or changing the forms of drugs (amorphous/ester/salt/cocrystal, etc.) (Sinha et al. 2010; Kalepu and Nekkanti 2015). The solid dispersion (SD) technique has been widely employed in the pharmaceutical industry to improve the oral bioavailability of BCS Class II and Class IV compounds by improving their kinetic aqueous solubility (Shah et al. 2013; Zhang et al. 2017; Ellenberger et al. 2018; Meng et al. 2021). Physically, SDs are eutectic mixtures or solid solutions in which drug molecules exist either as amorphous or as microcrystal forms dispersed in the carrier. Compared with the crystalline forms of drugs, the amorphous/microcrystal forms dispersed in the proper carrier have higher free energy, which helps overcome the lattice energy in the process of dissolution. Meanwhile, the solubilization effect of the polymer could be helpful for the solubility of small molecules. The dissolution rate of small molecules in aqueous solution can be significantly increased, and a high supersaturation state of the drug can be maintained for a long duration (Leuner and Dressman 2000; Yu 2001). Moreover, the polymers could help to maintain a thermodynamically more stable amorphous form during the manufacturing process, storage, and dosing process, especially to stabilize the metastable state by preventing nucleation (Yu 2001; Yu et al. 2015).

The antitumor drug candidate (E)-N-(4-bromophenyl)-3-(7-hydroxy-4-oxo-4H-chromen-3-yl)acrylamide (laboratory code X-05) (Fig. 1), which is a light yellow crystalline powder, is being developed as an innovative anti-lung cancer drug due to its excellent antitumour activity (Zhang et al. 2013). A Caco-2 cell permeability study and solubility study confirmed that X-05 is a BCS class II or IV compound (Table 1). Therefore, a major challenge is to develop appropriate preparations for preclinical studies and further clinical phase research.

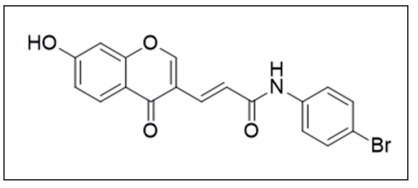

Fig. 1: The structure of X-05.

Table 1: Physicochemical properties of X-05

Physicochemical properties	**X-05**			
BSC Class	II or IV			
Melting point	DSC result showed a single endothermic peak at the onset of 277.5°C.			
Aqueous solubility at pH 1[a]	0.7 µg /mL			
Aqueous solubility at pH 7[a]	0.09 µg /mL			
Aqueous solubility at pH 9[a]	0.2 µg /mL			
Permeability[b]	Conc. (µM)	+/- GF120918 (Conc. 10µM)[c]	Mean P_{app} ($\times 10^{-6}$ cm/s)	
			A to B	B to A
	2	-	0.63	8.93
		+	1.80	1.51
	5	-	0.81	10.14
		+	2.11	1.68

a: Supplementary Information, Table S1.
b: Supplementary Information, Table S4.
c: A potent inhibitor of efflux transporter(s), such as P-glycoprotein (P-gp) and Breast Cancer Resistance Protein (BCRP).

In this study, by evaluating the preliminary results of kinetic solubility in biorelevant media (Supplementary Information, Figure S2) and the structural analysis of eight polymers and X-05, some polymers, which may have intermolecular interactions with X-05, were chosen to select a suitable carrier for X-05 to prepare amorphous solid dispersions (ASDs). One proper polymer was selected and the drug-polymer interactions of the optimum polymer with X-05 were studied by ultraviolet spectrophotometry (UV) (Nie et al. 2015; Nie et al. 2016), nuclear magnetic resonance spectrometry (NMR) (Nie et al. 2015; Li et al. 2019; Que et al 2019), infrared (IR) and Raman spectroscopy (Meng et al. 2015; Yu 2015; Zhang et al. 2017; Shi et al. 2019; Okada et al. 2020).

2. Investigations, results and discussion

X-05 ASDs were prepared by spray drying with Kollidon® 30 (PVP K30), Kollidon® VA 64 (PVP VA 64) and hypromellose acetate succinate (AquaSolve MG) (HPMCAS). This section is divided into four parts. First, we discuss the characterization of X-05 ASDs in different polymers with polarized light microscopy (PLM), X-ray powder diffraction (XRPD) and thermal analysis; next, we discuss the kinetic solubility of X-05 ASDs in Fasted State Simulated Intestinal Fluid (FaSSIF), Fed State Simulated Intestinal Fluid (FeSSIF), and Simulated Gastric Fluid (SGF); then, we discuss the solid-state stability of X-05 ASDs in high temperature/humidity for as long as four weeks; last, we discuss the interactions between the molecules of X-05 and PVP VA 64 to understand the stabilization of X-05 in PVP VA 64 with high drug loading.

2.1. PLM images

From the PLM images (Fig. 2), we can see that X-05 is an acicular crystalline material with a length of approximately 20~40 µm. There was no birefringence of ASDs X-05-PVP K30, X-05-PVP VA 64 and X-05-HPMCAS.

2.2. XRPD

Although there are some methods to detect the crystalline forms of drugs in ASDs, XRPD remains the gold standard method to detect the crystallinity of a drug within ASDs. XRPD can measure the diffraction of X-rays on the solid sample, and the diffraction pattern of the ASD is diffuse, whereas the diffraction pattern of the crystal shows some characteristic sharp diffraction peaks.
The XRPD pattern for crystalline X-05 shows multiple strong distinct peaks at 11.129, 15.184, 17.009, 19.720, 24.545, 24.805 and 34.296° 2θ (Fig. 3a). The presence of sharp, distinctive peaks for crystalline X-05 in the XRPD makes it relatively easy to identify the presence of crystalline X-05 in ASDs. As shown in Fig. 3,

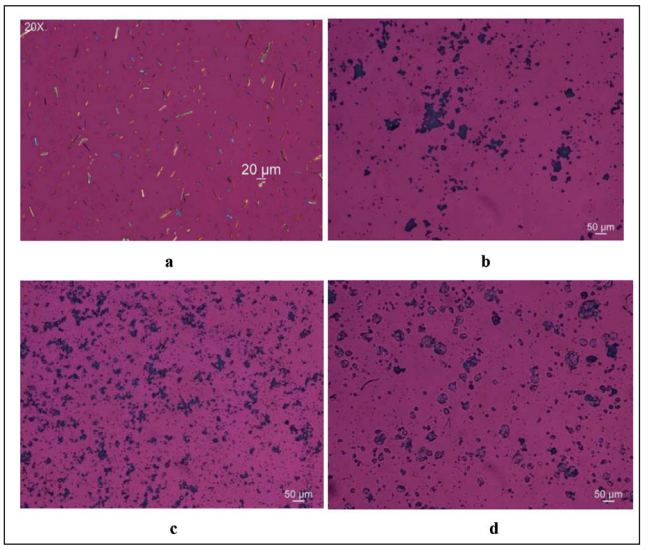

Fig. 2: PLM images of (a) X-05, (b) ASD X-05-PVP K30 (20% DL), (c) ASD X-05-PVP VA 64 (20% DL) and (d) ASD X-05-HPMCAS (20% DL).

the disappearance of all sharp peaks characteristic of crystalline X-05 following spray drying confirmed the amorphous nature of the ASDs in each polymer tested. Even though the intensity of these diffractograms was not strong enough, the PLM pictures and DSC results were strong evidence for amorphous forms as well.

2.3. Thermal analysis

The measurement of glass transition temperature (T_g) is considered to be the "gold standard" to evaluate miscibility in ASDs (Huang and Dai 2014; Paudel et al. 2014). The melting point of X-05 was 277.5 °C and approximately 1.24% of the weight loss may be due to the melting of X-05 (Fig. 4a). Differential scanning calorimetry (DSC) cycle results showed that the T_g of pure X-05 was approximately 131 °C (Fig. 4b). The modulated DSC (MDSC) results indicated that single T_g of ASDs X-05-PVP K30, X-05-PVP VA 64 and X-05-HPMCAS were present, which were approximately 174.6 °C, 109.0 °C and 114.3 °C, respectively (Fig. 4c, d, e), and indicated good miscibility between X-05 and polymers.

2.4. Kinetic solubility of X-05 and ASDs in FaSSIF, FeSSIF and SGF

The results show that the kinetic solubilities of ASDs X-05-PVP K30, X-05-PVP VA 64 and X-05-HPMCAS in FaSSIF were

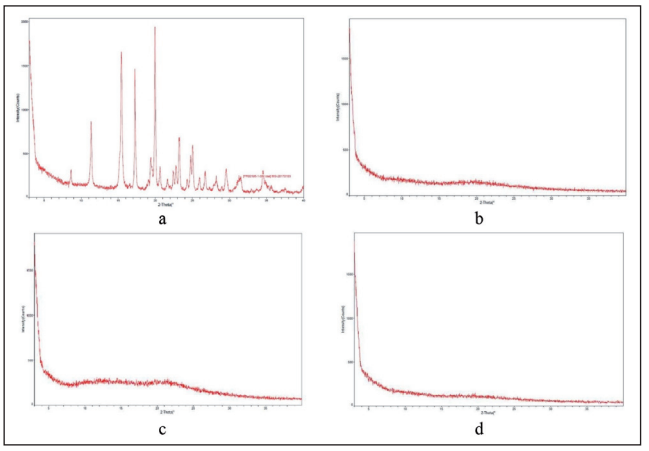

Fig. 3: XRPD patterns of (a) X-05, (b) ASD X-05-PVP K30 (20% DL), (c) ASD X-05-PVP VA 64 (20% DL) and (d) ASD X-05-HPMCAS (20% DL).

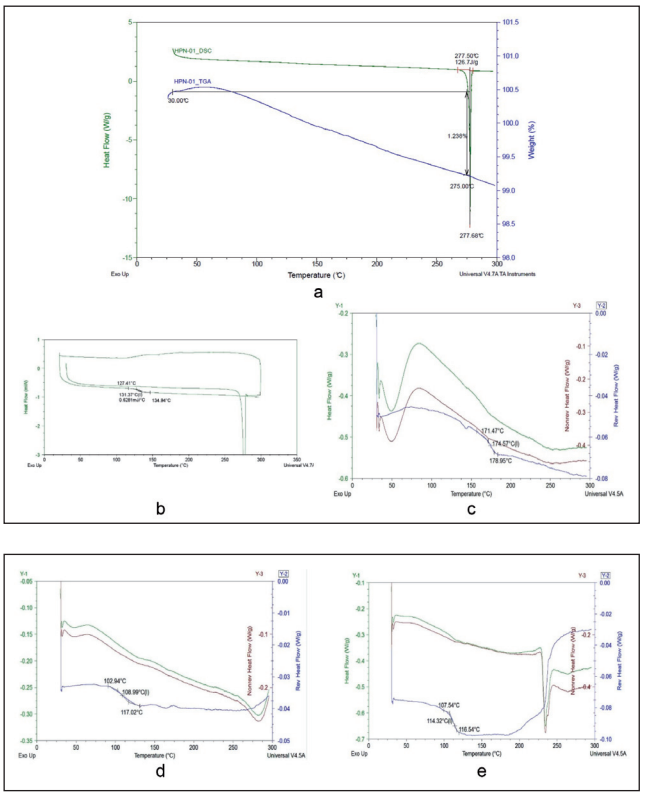

Fig. 4: (a) DSC and TGA patterns of crystal X-05; (b) DSC pattern of amorphous X-05; MDSC of (c) ASD X-05-PVP K30 (20% DL), (d) ASD X-05-PVP VA 64 (20% DL) and (e) ASD X-05-HPMCAS (20% DL).

approximately 5, 15 and 16 times higher than that of crystalline X-05 for 180 min. However, the solubilization rate of X-05-HPMCAS in FaSSIF was slower than that of X-05-PVP VA 64 within 2 hours, while the solubilization effect of PVP K30 on X-05 in FaSSIF was very weak. The kinetic solubilities of ASDs X-05-PVP K30, X-05-PVP VA 64 and X-05-HPMCAS in FeSSIF were approximately 5, 5 and 2 times higher than that of crystalline X-05 for 180 min. Compared with the results in FaSSIF, the solubilities of ASDs X-05-PVP K30, X-05-PVP VA 64, X-05-HPMCAS and crystalline X-05 in FeSSIF were increased by 13, 4, 2 and 14 times for 180 min, respectively. All the results indicated that the solubility of X-05 in ASDs and crystalline X-05 in the gastrointestinal tract may be affected by food. The kinetic solubilities of ASDs X-05-PVP K30, X-05-PVP VA 64 and X-05-HPMCAS in SGF were approximately 11, 3 and 4 times higher than that of crystalline X-05 for 180 min. Since drug absorption over the gastric wall is negligible, the solubility in FaSSIF is the most important reference for polymer selection. Therefore, PVP VA 64 has the best solubilization effect, and the solubility of ASD X-05-PVP VA 64 may have a lower food effect. The kinetic solubility results of the three ASDs in FaSSIF, FeSSIF and SGF at 37 °C are illustrated in Fig. 5 to Fig. 7, and that of X-05 is shown as a control.

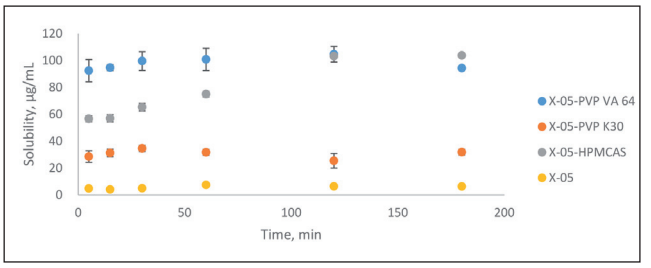

Fig. 5: Kinetic solubility results of ASDs (20% DL) and X-05 in FaSSIF at 37 °C. Each vail contained equivalent to approximately 3 mg of X-05 in 6 mL of FaSSIF. The concentration of the clear solution was tested at 5, 15, 30, 60, 120, and 180 minutes after stirred in a thermomixer at 37 ºC under 600 rpm. Three replicates were prepared for each sample.

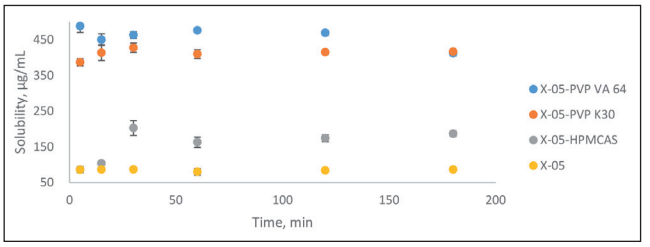

Fig. 6: Kinetic solubility results of ASDs (20% DL) and X-05 in FeSSIF at 37 °C. Each vail contained equivalent to approximately 3 mg of X-05 in 6 mL of FeSSIF. The concentration of the clear solution was tested at 5, 15, 30, 60, 120, and 180 minutes after stirred in a thermomixer at 37 ºC under 600 rpm. Three replicates were prepared for each sample.

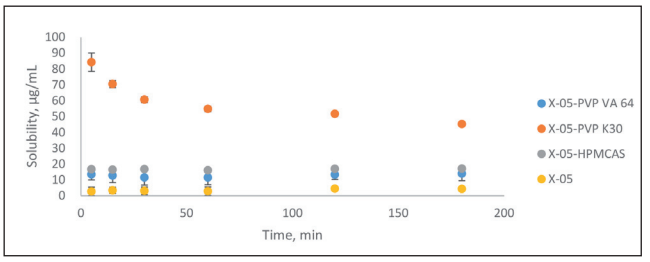

Fig. 7: Kinetic solubility results of ASDs (20% DL) and X-05 in SGF at 37 °C. Each vail contained equivalent to approximately 3 mg of X-05 in 6 mL of SGF. The concentration of the clear solution was tested at 5, 15, 30, 60, 120, and 180 minutes after stirred in a thermomixer at 37 ºC under 600 rpm. Three replicates were prepared for each sample.

2.5. *Solid-state stability*

ASD samples with PVP K30 (20% DL), PVP VA 64 (20% DL) and HPMCAS (20% DL) were exposed to 40 °C and 75% relative humidity (40 °C/75% RH) and 60 °C/ambient RH for short-term stability studies.

From the stability data (Supplementary Information, Table S6 & Table S7) and HPLC chromatograms (Fig. 8 & Fig. 9), we could see that a new impurity RRT 0.95 in ASD X-05-PVP K30 was generated with peak areas of 0.07% and 0.19% when the ASD samples were stored at 40 °C/75% RH and 60 °C/ambient RH for a week. The same impurity could also be found in ASD X-05-HPMCAS with a peak area of 0.14% at the initial time point. The impurity RRT 0.95 in ASD X-05-HPMCAS was increased to 0.21% and 0.23% after one week of storage at 40 °C/75% RH and 60 °C/ambient RH, respectively. Furthermore, in ASD X-05-HPMCAS, another impurity RRT 0.98 was found, which increased to 0.09% and 0.30% after one week of

storage at 40 °C/75% RH and 60 °C/ambient RH, respectively. Based on the above stability data, it was confirmed that ASD X-05-PVP VA 64 was the most stable form among the three ASDs.

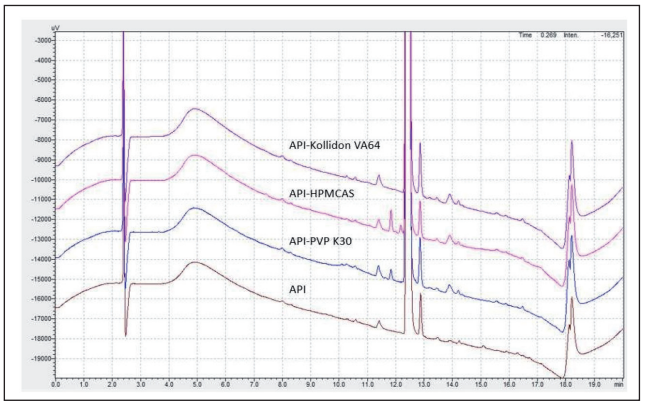

Fig. 8: HPLC chromatograms of ASDs (20% DL) for up to 1 week (40 °C/75% RH).

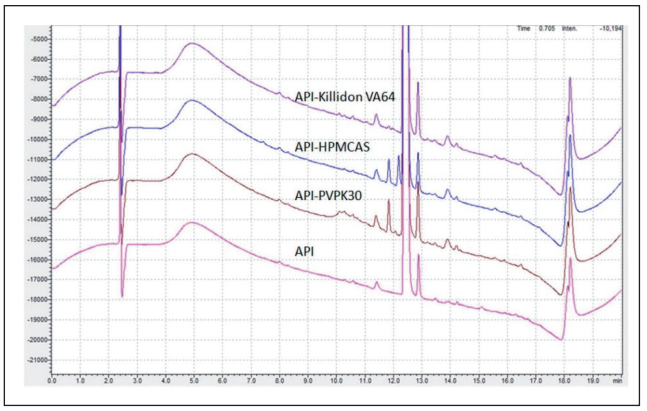

Fig. 9: HPLC chromatograms of ASDs (20% DL) for up to 1 week (60 °C/ambient RH).

HPMCAS is a mixture of acetic acid and monosuccinic acid esters of hydroxypropyl methylcellulose, which is a cellulose-based enteric coating polymer with a T_g of 113 °C and the average molecular weight is in the range of 55000~90000 (Baghel et al. 2016). It can be dissolved in methanol or acetone but is insoluble in ethanol or water (Chavan et al. 2019). The hydroxyl groups in HPMCAS can form hydrogen bonds with electronegative groups such as oxygen and nitrogen in drug molecules and enhance the solubility of poorly water-soluble drugs. Although HPMCAS has great potential in enhancing the solubility of poorly water-soluble drugs, it probably undergoes hydrolysis at high temperature during manufacturing and releases acetic acid and succinic acid, which can react with the hydroxyl groups in the active pharmaceutical ingredient (API) and form esters, thereby causing drug-excipient incompatibilities (Newman 2015; Yu et al. 2015). In this case, the existence of a carboxylic acid residue in the monosuccinic acid ester block might be the main cause of the impurity RRT 0.95, which was found at the initial point in the stability study. It may be one of the degradation byproducts of the hydrolysis reaction of the amido bond of X-05 induced by the enriched carboxyl group in HPMCAS polymer molecules.

PVP K30 is a nonionic polymer with a T_g of approximately 164 °C (Shi et al. 2019), and the average molecular weight is in the range of 44000~54000. PVP VA 64 is a copolymer of 1-vinyl-2-pyrrolidone and vinyl acetate in a ratio of 6:4 (m/m) with a T_g of 103 °C to 106 °C, and the average molecular weight is in the range of 45000~70000 and readily dissolves in all hydrophilic solvents (Newman 2015). The stability of X-05 in PVP K30 and PVP VA 64 is better than that of ASD in HPMCAS. The unit structure of PVP K30 is obviously different from that of PVP VA 64. In polymer PVP VA 64, both the VP units and the VA units are hydrogen bond acceptors because there are -C=O groups in the VP and VA units, and the formation of hydrogen bonds with drugs containing proton donors could stabilize amorphous drug substances (Yu et al. 2015; Dean et al. 2019). Due to the existence of VA units, the relative distance of VP units, which are a kind of rigid group in the PVPVA polymer, is slightly longer than that in the PVP polymer, so PVP VA64 is a more flexible polymer than PVP K30. The lack of flexible acetyl units may result in weak interactions between X-05 and steric resistance and rigid pyrroline, showing high intermolecular mobility, and the sensitive groups of X-05 are more susceptible to degradation under the influence of temperature and humidity. The flexibility and the more kinds of hydrogen bond acceptors make PVP VA64 a more suitable polymer for X-05.

Other stability studies of ASD samples with PVP VA 64 (30% DL, 40% DL and 50% DL) were performed for as long as four weeks at 40 °C/75% RH (Supplementary Information, Table S8) and 60 °C/ambient RH (Supplementary Information, Table S9). The XRPD results show that all the ASDs remained amorphous over 4 weeks (Fig. 10), and there was no significant change in purity for all the ASDs. For ASD X-05-PVP VA 64 with 40% DL and 50% DL, the impurity RRT 1.04 was increased slightly under 40 °C/75% RH (from 0.40% to 0.44% and 0.50%) and 60 °C/ambient RH (from 0.40% to 0.45% and 0.52%). The reason might be that a higher drug loading with higher API concentration and higher mobility of X-05 molecules are more susceptible to the influence of environmental temperature and humidity. The above results indicate that PVP VA 64 would be the most efficient carrier to form an ASD with X-05 due to its superior drug loading capacity and better physical stability.

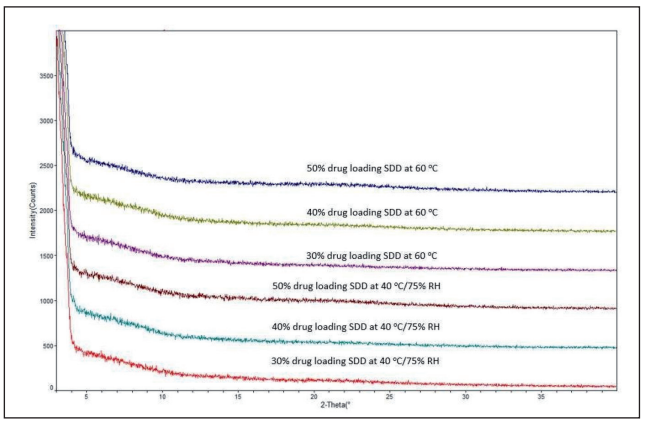

Fig. 10: XRPD patterns of ASDs X-05-PVP VA 64 for up to 4 weeks. (**Note:** from top to bottom: 50% DL at 60 °C/ambient RH, 40% DL at 60 °C/ambient RH, 30% DL at 60 °C/ambient RH, 50% DL at 40 °C/75% RH, 40% DL at 40 °C/75% RH and 30% DL at 40 °C/75% RH)

2.6. UV spectroscopy

To confirm whether the dispersion of X-05 in PVP VA 64 would cause significant changes in the backbone of the molecule, UV detection of X-05, PVP VA 64 and X-05-PVP VA 64 ASD (40% DL) was carried out. As shown in Fig. 11, the UV spectrum of PVP VA 64 shows a single UV absorption peak at 195.60 nm since only carbonyl groups (amide and ester groups) are present in the polymer molecule. Three chromophores in X-05, the carbonyl group, trans-double bond and benzene ring, contribute four strong to medium strength UV absorption peaks at 357.30 nm, 293.20 nm, 239.20 nm and 196.10 nm. The UV spectrum of ASD X-05-PVP VA 64 (40% DL) shows exactly the same absorption peaks as that of X-05, which means that X-05 contributes the main absorption of the ASD sample. The comparison of the UV absorption of X-05 and ASD X-05-PVP VA 64 (40% DL) indicated that the backbone of the X-05 molecule in ASD has not undergone any changes.

2.7. NMR spectroscopy

X-05, PVP VA 64 and ASD X-05-PVP VA 64 (40% DL) were detected by NMR using DMSO-d_6 as the solvent (Fig. 12). Except

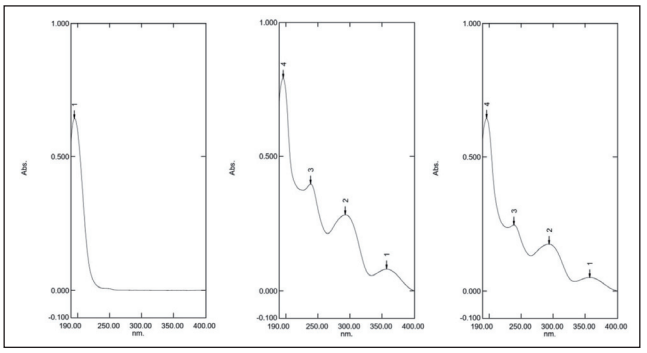

Fig. 11: UV spectra of PVP VA 64, X-05 and ASD X-05-PVP VA 64 (40% DL) from left to right.

for the solvent peak at 2.5 ppm and water peak at 3.3 ppm, a strong absorption of methyl on the acetyl group at 1.8 ppm was observed from the PVP VA 64 sample. At 1.6 ppm and 2.05 ppm, there are two groups of medium-strong absorption peaks corresponding to hydrogen atoms on pyrrolidone units in the structure of PVP VA 64. The moderate intensity absorption peak near 3.1 ppm corresponds to the hydrogen atom on the carbon connected with the oxygen and nitrogen atoms on the backbone chain of the polymer. By comparing with the NMR data of two single components, the two components of ASD X-05-PVP VA 64 dissolved in DMSO-d_6 showed relative independence, and the positions of the peak of hydrogen atoms in the two molecules do not show any displacement, disappearance or increase in the magnetic field. Although ASD is prepared by polymer and X-05, intermolecular interactions are unlikely to occur in DMSO when the two components are relatively far apart or completely solubilized.

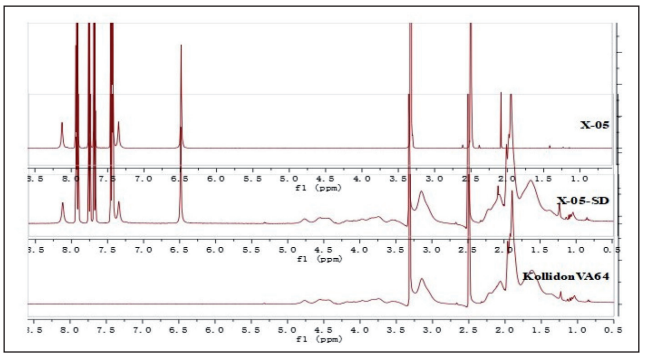

Fig. 12: 1D ^{1}H spectra for X-05, ASD X-05-PVP VA 64 (40% DL) and PVP VA 64 in DMSO-d_6, 298 K.

2.8. *IR spectroscopy*

The intermolecular interactions between X-05 and PVP VA 64 in ASD X-05-PVP VA 64 (40% DL) were investigated using IR.

For ASD X-05-PVP VA 64 (40% DL), in the high-frequency region of 3000-3500 cm^{-1}, the strong absorption peak of -OH and -NH stretching vibrations in X-05 weakens to a medium-strong peak, which appears in the form of a shoulder peak on the right side of the signature absorption peak of the polymer in this region. In the mid-frequency region of 1600~1800 cm^{-1} of the IR spectrum, 1) the strong absorption peaks of the two O=C stretching vibrations of PVP VA 64 shifts in the spectrum of ASD X-05-PVP VA 64 (40% DL) from 1735.93 cm^{-1} to 1734.01 cm^{-1}. 1676.14 cm^{-1} redshifts to 1662.64 cm^{-1}. 2) The strong absorption peak of the O=C stretching vibration of X-05 does not change and is still at 1654.92 cm^{-1} and 1618.28 cm^{-1} in the spectrum of ASD X-05-PVP VA 64 (40% DL). Only the absorption intensity decreases to a certain extent. The changes in the intensity or position of the two absorption peaks above suggest that the phenolic hydroxyl and amide nitro-hydride of X-05 and the two carbonyl groups in the structural unit of PVP VA 64 were involved in the hydrogen bond interaction between large and small molecules. As shown in Fig. 13, the two repeating units of PVP VA 64 are arranged in linear spacing. Due to steric hindrance, pyrrolidone and acetyl oxide groups are arranged in a three-dimensional (3D) spiral in the polymer. The dense carbonyl spacers form hydrogen bonds with the active hydrogen of X-05, slowing their free stretching vibration. However, both active hydrogens of X-05 participate in the formation of hydrogen bonds, so the free stretching vibration of active hydrogen is inhibited. Since other functional groups of polymer and X-05 did not participate in the interaction and were far away from each other in 3D space (Fig. 14), there was no influence on the in-plane and out-of-plane bending vibration and shear vibration, so the changes in peak height and position in the low-frequency fingerprint region of the IR spectrum are not obvious.

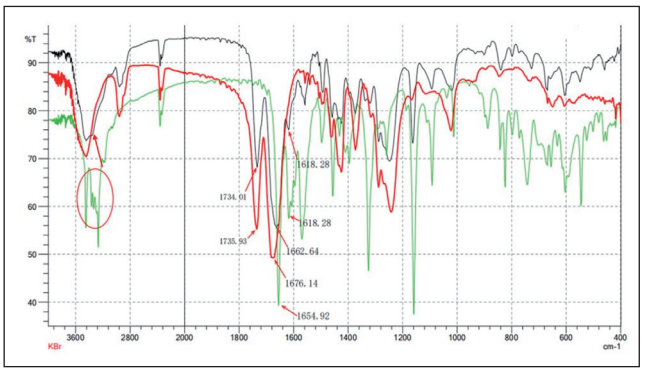

Fig. 13: IR spectra for X-05 (green), PVP VA 64 (red) and ASD X-05-PVP VA 64 (40% DL) (black).

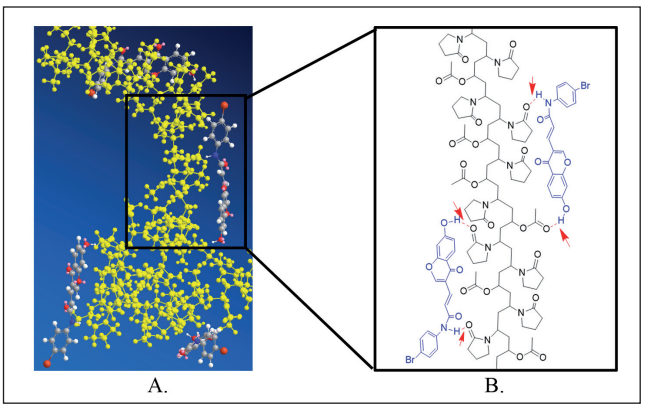

Fig. 14: Simulated molecular interactions between X-05 and PVP VA 64 (A. the 3D mode of the ASD X-05-PVP VA 64, of which the energy was minimized by the MM2 program in Chem3D; in which the backbone was marked yellow; B. the Zoom in picture of the part of the 3D structure)

2.9. *Raman spectroscopy*

Raman spectroscopy was employed to confirm the molecular interactions observed in IR and obtain complementary information to characterize changes associated with the formation of molecular interactions (Meng et al. 2015). Figure 15 shows Raman peaks of X-05, PVP VA 64 and ASD X-05-PVP VA 64 (40% DL). This result indicated that the peak positions of ASD X-05-PVP VA 64 were slightly shifted compared to those in X-05 and PVP VA 64. In the high frequency region of 2800-3100 cm^{-1}, the strong absorption peak of the -CH stretching vibration in PVP VA 64 weakens to a weak peak in ASD X-05-PVP VA 64, which may be due to the lower concentration and be affected by the existence of the X-05 molecule. In the middle frequency region, the two typical weak peaks at 1731.93 cm^{-1} and 1674.44 cm^{-1} of PVP VA 64 disappeared, which means that nearly both kinds of O=C were affected by the formation of hydrogen bonds between X-05 and the carbonyl of PVP VA 64 in ASD X-05-PVP VA 64. Additionally, the two typical peaks of X-05 at 1614.31 cm^{-1} and 1595.77 cm^{-1}

did not shift except for a certain extent of weakness. These results agreed with those of the IR spectrum, which proved the formation of hydrogen bonds between the polymer and small molecules.

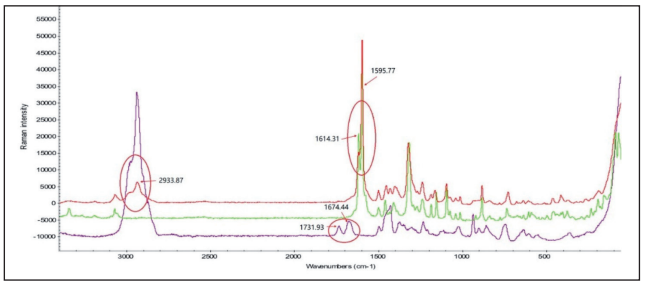

Fig. 15: Raman spectra for X-05 (green), PVP VA 64 (purple) and ASD X-05-PVP VA 64 (40% DL) (red).

3. Conclusions

The advantages of ASD make it one of the most widely used and successful techniques in formulation development. ASD can enhance the aqueous solubility of poorly water-soluble drugs and may improve the solid stability of drug candidates. Its solid-state allows for greater flexibility in formulation dosage design, product manufacturing, storage and transportation.

In this case, by studying the kinetic solubility and solid-state stability of ASDs prepared with different polymers, we are able to screen the most suitable polymer, and this approach is expected to simplify the time-consuming polymer screening process using proper design strategies. An amorphous solid dispersion system of X-05 in PVP VA 64 was found to have superior drug loading (50%) capacity and better physicochemical stability due to strong drug-polymer interactions. The X-05 ASD in PVP VA 64 may exhibit faster *in vitro* dissolution than the X-05 preparation. The drug-polymer interactions of PVP VA 64 with X-05 were studied by UV, NMR, and IR and Raman spectroscopy, and the results indicated that the intermolecular hydrogen bond interaction between the drug and polymer was the foundation of the solubilization and stabilization of X-05 in PVP VA 64, which also contributed to the high drug loading and stability over a long duration. The results provide the theoretical basis for the establishment of a control strategy and specifications of the product intermediates. Therefore, ASD X-05-PVP VA 64 is expected to solve the problems of insufficient dosage and low exposure in vivo for PK studies and toxicity evaluation, as well as the development of oral solid preparations for early clinical trials.

4. Experimental

4.1. Materials

X-05 was synthesized in the laboratory. Kollidon® 30 (PVP K30) and Kollidon® VA 64 (PVP VA 64) were obtained from BASF SE (Ludwigshafen, Germany). Hypromellose acetate succinate (AquaSolve MG) (HPMCAS) was obtained from Ashland (Schaffhausen, Switzerland). SIF powder was obtained from Biorelevant (London, United Kingdom). HPLC-grade acetonitrile was purchased from Fisher Scientific (Pittsburgh, PA, USA). All other chemicals used in this study were analytical grade or higher.

4.2. Methods

4.2.1. Preparation of ASDs of X-05

Spray-dried ASDs X-05-PVP K30, X-05-PVP VA 64 and X-05-HPMCAS at 20% drug loading (DL) were prepared on a ProCepT 4M8-TriX spray dryer (Zele, Belgium). Briefly, X-05 and PVP K30 or PVP VA 64 were dissolved in a tetrahydrofuran (THF)/water (1:1, v/v) cosolvent at a total solid concentration of 50 mg/mL. X-05 and HPMCAS were dissolved in THF at a total solid concentration of 100 mg/mL. The solutions were then sprayed at a pump speed of 400 rpm. The drying air was maintained at a flow rate of 0.3 m^3/min with inlet and outlet temperatures of 95 °C and 51 °C, respectively. The cooling air flow was 0.2 m^3/min. The samples were dried overnight under vacuum at room temperature.

Spray-dried ASD X-05-PVP VA 64 at 30%, 40% and 50% DL were prepared on a ProCepT 4M8-TriX spray dryer (Zele, Belgium). Briefly, X-05 and PVP VA 64 were dissolved in a THF/water (1:1, v/v) cosolvent with a concentration of X-05 at 20 mg/mL for 30% and 40% DL and at 16.67 mg/mL for 50% DL. The following operation parameters were the same as previously described.

4.2.2. PLM

A Nikon LV100POL microscope equipped with a 5 megapixel CCD and a 20X physical lens was used.

4.2.3. XRPD

To confirm the amorphous state of the microparticles, all prepared samples were characterized by XRPD (Bruker, D8 Advance) equipped with a Cu Kα source (40 kV, 40 mA), and the sample rotation speed was 15 rpm at a scanning speed of 10°/min over an angular range of 2θ of 3°-40°.

4.2.4. Thermal analysis

4.2.4.1. DSC

The thermal properties of X-05 and the three ASDs were characterized using DSC (TA Instruments, DSC Q2000). The thermal behavior of pure X-05 was characterized by heating-cooling-heating cycles. Samples were heated at 10 °C/min from 30 to 300 °C (Cycle 1), cooled at a rate of 10 °C/min to 30 °C (Cycle 2), and then reheated at 10 °C/min to 300 °C (Cycle 3). ASDs were modulated by MDSC at 1 °C every 60 s with a heating rate of 2 °C/min from 30 to 300 °C.

4.2.4.2. Thermal analysis system (TGA)

The weight loss of X-05 was measured by TGA (TA Instruments, TGA Q5000IR). Approximately 4 mg of X-05 was placed in an open platinum pan and heated from 30 °C to 300 °C at a rate of 10 °C/min under 25 mL/min of N_2.

4.2.5. Determination of the kinetic solubility of X-05 and ASDs in FaSSIF, FeSSIF and SGF

The biorelevant media FaSSIF, FeSSIF and SGF were prepared from SIF powder according to the instructions, which were developed to simulate the condition in the intestine in the fasted state, in the fed state and the condition in the stomach, respectively. To determine the most suitable carrier for X-05, kinetic solubility studies with different carriers such as PVP K30, PVP VA 64 and HPMCAS in FaSSIF, FeSSIF and SGF were carried out.

Approximately 3 mg of X-05 and three ASDs (equivalent to approximately 3 mg of X-05) were weighed into an 8 mL vial, and 6 mL of each biorelevant medium was added (target concentration 0.5 mg/mL). Then, the suspensions were stirred in a thermomixer at 37 ºC under 600 rpm. Two hundred microliters of suspensions were withdrawn at 5, 15, 30, 60, 120, and 180 min and then centrifuged at 14000 rpm for 5 min. After that, 100 µL of supernatant was diluted four times with acetonitrile (ACN)/water (1/1, v/v) to prevent precipitation, and the concentration was analyzed by the HPLC concentration method. Three replicates were prepared for each sample.

4.2.6. HPLC concentration method

All samples were diluted with ACN/water (1/1, v/v) to a concentration of 0.1 mg/mL. HPLC analysis was carried out on a Shimadzu LC-20ADXR system using a Waters Atlantis® T3 column (150 mm × 4.6 mm, 3.0 µm) at 40 °C with a flow rate of 1 mL/min and detection at 240 nm for 8 min. The mobile phase involved an aqueous solution (water containing 0.1% trifluoroacetic acid (TFA), v/v) as phase A and ACN as phase B. The HPLC analyses were accomplished with a gradient elution program (time (min)/ % B: 0/5, 4/95, 4.01/5 and 8/5).

4.2.7. Solid-state stability study

ASDs X-05-PVP K30, X-05-PVP VA 64 and X-05-HPMCAS were stored at 40 °C/75% RH and 60 °C/ambient RH for one week. ASD samples with PVP VA 64 (30% DL, 40% DL and 50% DL) were stored under the same conditions mentioned above for as long as 4 weeks. The purities of each sample at the initial time point, 1 week and 4 weeks were analyzed by the HPLC purity method.

4.2.8. HPLC purity method

All samples were diluted with ACN/water (1/1, v/v) to a concentration of 0.1 mg/mL. HPLC analysis was carried out on a Shimadzu LC-20ADXR system using a Waters Atlantis® T3 column (150 mm × 4.6 mm, 3.0 µm) at 40 °C with a flow rate of 1 mL/min and detection at 240 nm for 20 min. The mobile phase involved an aqueous solution (water containing 0.1% TFA, v/v) as phase A and ACN as phase B. The HPLC analyses were accomplished with a gradient elution program (time (min)/ % B: 0/5, 15/95, 15.1/5 and 20/5).

4.2.9. UV spectroscopy

X-05, PVP VA 64 and ASD X-05-PVP VA 64 were diluted with ACN to a concentration of 0.5 mg/mL. The UV spectra of the solutions were recorded on a Shimadzu UV-2600 UV-Vis spectrophotometer. The wavelength range was set from 190 to 400 nm.

4.2.10. NMR spectroscopy

1D ^{1}H NMR spectra were acquired on a Bruker 400 MHz Avance-III spectrometer equipped with a 5 mm BBOF probe with Z-axis gradients at 25 °C using standard

sequences. Approximately 10 mg of X-05, PVP VA 64 and ASD X-05-PVP VA 64 were transferred to 5 mm NMR tubes, and then 0.5 mL of fresh deuterated dimethyl sulfoxide (DMSO-d_6) was added to dissolve the powder for NMR data acquisition.

4.2.11. IR spectroscopy

FT-IR spectra of the solid X-05, PVP VA 64 and ASD X-05-PVP VA 64 were measured using a Shimadzu IRtracer-100 Fourier transform IR spectrometer using KBr disks. Analysis of the spectra was performed using LabSolutions IR software.

4.2.12. Raman spectroscopy

Raman spectra of the solid X-05, PVP VA 64 and ASD X-05-PVP VA 64 were measured using a Raman Imaging Microscope (Thermo Scientific, DXR2xi) at an excitation wavelength of 532 nm and a laser power of 6 mW. The spectra were acquired in the scan range from 50 to 3500 cm^{-1} at a resolution of 4 cm^{-1} with 0.001 s of exposure and 1 scan at room temperature.

Acknowledgments: The authors gratefully acknowledge Hua Medicine for graciously providing the permission to use the ChemOffice 2017 software.

Disclosure statement: There are no relevant financial or non-financial competing interests to report.

References

Amidon GL, Lennernas H, Shah VO, Crison JR (1995) A theoretical basis for a biopharmaceutic drug classification: the correlation of in vitro drug product dissolution and in vivo bioavailability. Pharm Res 12: 413–420.

Baghel S, Cathcart H, O'Reilly NJ (2016) Polymeric amorphous solid dispersions: a review of amorphization, crystallization, stabilization, solid-state characterization, and aqueous solubilization of biopharmaceutical classification system class II drugs. J Pharm Sci 105: 2527–2544.

Chavan RB, Rathi S, Jyothi VGSS, Shastri NR (2019) Cellulose based polymers in development of amorphous solid dispersions. Asian J Pharm Sci 14: 248–264.

Cook D, Brown D, Alexander R, March R, Morgan P, Satterthwaite G, Pangalos MN (2014) Lessons learned from the fate of AstraZeneca's drug pipeline: a five-dimensional framework. Nat Rev Drug Discov 13: 419–431.

Dean H, David C, Lawrence YFN, Mark D, Gavin MW, John GL, Clement LH (2019) An investigation of the inter-molecular interaction, solid-state properties and dissolution properties of mixed copovidone hot-melt extruded solid dispersions. J Drug Deliv Sci Technol 53:101132.

Ellenberger DJ, Miller DA, Kucera SU, Williams RO (2018) Improved vemurafenib dissolution and pharmacokinetics as an amorphous solid dispersion produced by KinetiSol® processing. AAPS PharmSciTech 19:1957–1970.

Huang Y, Dai W (2014) Fundamental aspects of solid dispersion technology for poorly soluble drugs. Acta Pharm Sin B 4: 18–25.

Kalepu S, Nekkanti V (2015) Insoluble drug delivery strategies: review of recent advances and business prospects. Acta Pharm Sin B 5: 442–453.

Leuner C, Dressman J (2000) Improving drug solubility for oral delivery using solid dispersions. Eur J Pharm Biopharm 50: 47–60.

Li Q, Zhao Q, Jing Q, Ma X, Chen N, Ren G, Ouyang D, Ren F (2019) Investigating molecular interactions of high-loaded glipizide-HPMCAS microparticles by integrated experimental and modeling techniques. Eur J Pharm Sci 131: 127–135.

Meng F, Ferreira R, Su Y, Zhang F (2021) A novel amorphous solid dispersion based on drug–polymer complexation. Drug Deliv Transl Res 11: 2072–2084.

Meng F, Trivino A, Prasad D, Chauhan H (2015) Investigation and correlation of drug polymer miscibility and molecular interactions by various approaches for the preparation of amorphous solid dispersions. Eur J Pharm Sci 71: 12–24.

Newman A (2015) Pharmaceutical amorphous solid dispersions. Hoboken (NJ): John Wiley & Sons, Inc.

Niazi SK (2007) Handbook of preformulation: chemical, biological and botanical drugs. New York (NY): Informa Healthcare USA, Inc.

Nie H, Mo H, Zhang M, Song Y, Fang K, Taylor LS, Li T, Byrn SR (2015) Investigating the interaction pattern and structural elements of a drug-polymer complex at the molecular level. Mol Pharmaceut 12: 2459–2468.

Nie H, Su Y, Zhang M, Song Y, Leone A, Taylor LS, Marsac PJ, Li T, Byrn SR (2016) Solid-state spectroscopic investigation of molecular interactions between clofazimine and hypromellose phthalate in amorphous solid dispersions. Mol Pharmaceut 13: 3964–3975.

Noyes AA, Whitney WR (1897) The rate of solution of solid substances in their own solutions. J Am Chem Soc 12: 930–934.

Okada H, Ueda K, Yasuda Y, Higashi K, Inoue M, Ito M, Noguchi S, Kawakami K, Moribe K. (2020). Correlation between drug dissolution and resistance to water-induced phase separation in solid dispersion formulations revealed by solid-state NMR spectroscopy. Int J Pharmaceut 577: 119086.

Paudel A, Geppi M, Mooter GVD (2014) Structural and dynamic properties of amorphous solid dispersions: the role of solid-state nuclear magnetic resonance spectroscopy and relaxometry. J Pharma Sci 103: 2635–2662.

Que C, Lou X, Zemlyanov DY, Mo H, Indulkar AS, Gao Y, Zhang GGZ, Taylor LS (2019) Insights into the dissolution behavior of ledipasvir-copovidone amorphous solid dispersions: role of drug loading and intermolecular interactions. Mol Pharmaceut 16: 5054–5067.

Shah N, Iyer RM, Mair HJ, Choi DS, Tian H, Diodone R, Fähnrich K, Pabst-Ravot A, Tang K, Scheubel E, Grippo JF, Moreira SA, Go Z, Mouskountakis J, Louie T, Ibrahim PN, Sandhu H, Rubia L, Chokshi H, Singhal D, Malick W (2013) Improved human bioavailability of vemurafenib, a practically insoluble drug, using an amorphous polymer-stabilized solid dispersion prepared by a solvent-controlled coprecipitation process. J Pharm Sci 102: 967–981.

Shi X, Xu T, Huang W, Fan B, Sheng X (2019) Stability and bioavailability enhancement of telmisartan ternary solid dispersions: the synergistic effect of polymers and drug-polymer(s) interactions. AAPS PharmSciTech 20: 143.

Sinha S, Ali M, Baboota S, Ahuja A, Kumar A, Ali J (2010) Solid dispersion as an approach for bioavailability enhancement of poorly water-soluble drug ritonavir. AAPS PharmSciTech 11: 518–527.

Technical-Information_Kollidon-VA-64. [accessed 2022 May 22]. http://transchemcorp.com/wp-content/uploads/2017/09/Technical-Information_Kollidon-VA-64.pdf

Tran P, Pyo Y, Kim D, Lee S, Kim J, Park J (2019) Overview of the manufacturing methods of solid dispersion technology for improving the solubility of poorly water-soluble drugs and application to anticancer drugs. Pharmaceutics 11: 132.

Yu L (2001) Amorphous pharmaceutical solids: preparation, characterization and stabilization. Adv Drug Deliver Rev 48: 27–42.

Yu M, Ocando JE, Trombetta L, Chatterjee P (2015) Molecular interaction studies of amorphous solid dispersions of the antimelanoma agent betulinic acid. AAPS PharmSciTech 16: 384–397.

Zhang S, Sun M, Zhao Y, Song X, He Z, Wang J, Sun J (2017) Molecular mechanism of polymer-assisting supersaturation of poorly water-soluble loratadine based on experimental observations and molecular dynamic simulations. Drug Deliv Transl Res 7: 738–749.

Zhang W, Heinzmann D, Grippo JF (2017) Clinical pharmacokinetics of vemurafenib. Clin Pharmacokinet 56: 1033–1043.

Zhang Y, Zhong H, Lv Z, Zhang M, Zhang T, Li Q, Li K (2013) Anti-hepatitis B virus and anti-cancer activities of novel isoflavone analogs. Eur J Med Chem 62:158–167.

Supplementary material

Solubility measurement

Approximately 5 mg of X-05 was weighed into a 2 mL vial, and 1 mL of pH 1, pH 7 and pH 9 aqueous buffer were added, respectively. Then the suspensions were stirred in a thermomixer at 25ºC under 600 rpm for 24 hours, and centrifuged at 14000 rpm for 5 min. After that, 500 µL of supernatant was diluted twice with acetonitrile (ACN)/water (1/1, v/v), and the concentration was analyzed by the HPLC concentration method. Three replicates were prepared for each sample.

Table S1. Aqueous solubility of X-05 at different pH buffers

Buffer	Solubility (µg/mL) at 25 °C	Avg. Solubility (µg/mL) at 25 °C	RSD (%)
pH 1	0.68	0.7	3.8
	0.67		
	0.72		
pH 7	0.085	0.09	4.2
	0.092		
	0.091		
pH 9	0.18	0.2	3.3
	0.17		
	0.17		

Permeability study

The objective of this study was to determine the bidirectional permeability and efflux ratio of X-05 in Caco-2 cells. Caco-2 cells at passage number 41 were seeded on 96-well transport inserts and cultured for 23 days before being used for the transport experiment. X-05 was dosed bi-directionally at 2 and 5 µM with or without 10 µM GF120918, a potent inhibitor of efflux transporter(s), such as P-glycoprotein (P-gp) and Breast Cancer Resistance Protein (BCRP). Samples were taken at 0 and 120 minutes after incubation from both the donor and receiver chambers and analyzed by Ultra-high-performance liquid chromatography-tandem mass spectrometry (UPLC-MS/MS). In the absence of GF120918, at 2 and 5 µM dosing concentrations, X-05 showed the mean apparent permeability coefficient (P_{app}) values of 0.63 and 0.81×10^{-6} cm/s, respectively, in the apical to basolateral (A to B) direction, and 8.93 and 10.14×10^{-6} cm/s, respectively, in the basolateral to apical (B to A) direction. In the presence of GF120918, X-05 showed the mean P_{app} values of 1.80 and 2.11×10^{-6} cm/s, respectively, at the two tested dosing concentrations, in the A to B direction, and 1.51 and 1.68×10^{-6} cm/s, respectively, in the B to A direction.

Materials

Dexamethasome, elacridar (GF120918), estrone 3-sulfate potassium (E3S), metoprolol tartrate, nadolol and tolbutamide were obtained from Sigma-Aldrich (Shanghai, China). Digoxin was obtained from TCI (Shanghai, China). Fetal bovine serum (FBS) was obtained from Corning (Woodland, CA, USA). Penicillin-streptomycin solution was obtained from HyClone (Logan, UT, USA). Minimum essential medium (MEM), Hank's balanced salt solution (HBSS), 0.05% trypsin-EDTA and 2-[4-(2-hydroxyethyl)-1-piperazinyl]ethanesulfonic acid (HEPES) were obtained from Gibco (Grand Island, NY, USA). Dimethyl sulfoxide (DMSO) was obtained from J&K Scientific (Langfang, China).

Methods

Cell culture

Caco-2 cells, purchased from ATCC (Shanghai, China), were cultured in MEM medium, supplemented with 1% non-essential amino acids, 10% FBS, 1% penicillin-streptomycin solution, and incubated under 37±1°C with 5% CO_2/95% air and saturated humidity. When reached 80-90% confluency, cells were digested with 0.05% trypsin-EDTA, and the cell density was adjusted 1×10^5 /mL with fresh medium to 96-well multiwell insert system. Cells were cultured for 23 days with medium changed every 4-5 days.

Solution preparation

Transport buffer: HBSS with 10 mM HEPES, pH 7.40±0.05.
Stop solution: 500 nM of dexamethasome in ACN and 250 ng/mL of tolbutamide in ACN for test compound (X-05) and control compounds (digoxin, E3S, nadolol and metoprolol), respectively.

Transport assay

The cell culture medium in 96-well insert plate was removed and rinsed twice with pre-warmed transport buffer. Appropriate dosing and receiving solutions were applied to the donor and receiver chambers to initiate the transport assay in A to B or B to A directions (75 and 250 µL for apical and basolateral wells, respectively). X-05 was tested at 2 and 5 µM in the presence or absence of 10 µM GF120918 bidirectionally in triplicate. Digoxin (P-gp substrate) was tested at 10 µM and E3S (BCRP substrate) was tested at 5 µM in the presence or absence of 10 µM GF120918 bidirectionally as well, while nadolol (low permeability control) and metoprolol tartrate (high permeability control) were tested at 2 µM in the absence of GF120918 in the A to B direction in triplicate. The plate was incubated for 2 hours in CO_2 incubator at 37±1°C, with 5% CO_2 at saturated humidity without shaking.
The initial dosing solution was transferred and mixed with the transport buffer and stop solution as the T0 sample. After 120 minutes, terminal samples were collected from the donor and receiver side of each well, mixed with the transport buffer and stop solution for UPLC-MS/MS analysis.
To lyse the cells for the determination of recovery, the remaining transport solutions were removed by gently tapping the cell plate on a paper towel. Stop solution was added into the apical well and mixed by pipetting up and down for 5 times before the lysing sample was taken from each apical well.
All samples were vortexed and centrifuged at 3220 rpm at 20°C for 20 minutes. Appropriate volume of supernatant was transferred to 96-well analysis plates.

Cell monolayer integrity measurement

Six wells per 96-well plate were randomly selected for Lucifer Yellow rejection assay to determine the cell monolayer integrity at the same duration of test compounds. 75 µL of 100 µM Lucifer Yellow in transport buffer and 250 µL transport buffer were added to apical and basolateral chambers, respectively. After 120 minutes incubation, 20 µL of Lucifer Yellow samples were taken from the apical sides, followed by the addition of 60 µL of transport buffer. And then 80 µL of Lucifer Yellow samples were taken from the basolateral sides. The relative fluorescence unit (RFU) of Lucifer Yellow was measured at 425/528 nm (excitation/emission) with microplate reader.

UPLC–MS/MS conditions

The UPLC–MS/MS system consisted of a Waters Acquity UPLC system (Milford, USA) and an API 4000 triple-quadrupole source (Applied Biosystems Sciex, Toronto, Canada). X-05 and internal standard (IS) separation were performed on a Waters acquity UPLC HSS T3 C18 column (2.1 × 50 mm, 1.7 µm). The mobile phase consisted of acetonitrile (B)-water (A). The flow rate was 0.55 mL/min and the temperature of column was ambient. The gradient program was as follows: 0-0.2 min, 5% B; 0.2-1.0 min, 5%–55% B; 1.0–1.4 min, 55%–98% B; 1.4–1.8 min, 98% B; 1.8–2.2 min 5% B. The total run time was 2.2 min. The mass spectrometer was operated in positive ionization mode with multiple reaction monitoring (MRM). The ion source was IonDrive Turbo V, the DP value was 50 eV (X-05), 80 eV (IS, dexamethasome), and the collision energy (CE) was 40 eV (X-05), 13 eV (IS). The ion reaction for quantitative analysis was m/z 386.0→215 (X-05), m/z 393.0→373.1 (IS). Instrumental conditions for control compounds and IS are shown in Table S2 and S3.

Table S2: UPLC conditions for control compounds

Compound Name	Nadolol, Metoprolol tartrate				Digoxin				Estrone 3-sulfate potassium			
Mobile Phase A	0.1% Formic Acid in Water											
Mobile Phase B	0.1% Formic Acid in Acetonitrile											
Column	Waters Acquity UPLC BEH C18, 2.1 × 50 mm, 1.7 µm											
Internal Standard	Tolbutamide											
Injection Volume	Nadolol: 6 µL, Metoprolol: 3 µL				4 µL				2 µL			
Gradient	Time (min)	Flow Rate (mL/min)	A (%)	B (%)	Time (min)	Flow Rate (mL/min)	A (%)	B (%)	Time (min)	Flow Rate (mL/min)	A (%)	B (%)
	0.01	0.500	95	5	0.01	0.600	90	10	0.01	0.500	95	5
	0.80	0.500	5	95	0.80	0.600	2	98	0.20	0.500	95	5
	1.00	0.500	5	95	1.00	0.600	2	98	1.20	0.500	25	75
	1.01	0.500	95	5	1.01	0.600	90	10	1.50	0.500	25	75
	1.20	0.500	95	5	1.20	0.600	90	10	1.60	0.500	5	95
									1.80	0.500	5	95
									1.81	0.500	95	5
									2.00	0.500	95	5

Table S3: MS conditions for control compounds

Compound Name	Nadolol, Metoprolol				Digoxin				Estrone 3-sulfate potassium			
Ion Source	ESI											
Scan Type	MRM											
Polarity	Positive				Negative				Negative			
Analyte	Ion Transition (m/z)	Retention Time (min)	DP (eV)	CE (eV)	Ion Transition (m/z)	Retention Time (min)	DP (eV)	CE (eV)	Ion Transition (m/z)	Retention Time (min)	DP (eV)	CE (eV)
	Nadolol: 310.354/254.044	0.56	65	25	Digoxin: 825.6/779.6	0.67	-82	-33	E3S: 349.1/269.0	1.19	-93	-40
	Metoprolol tartrate: 268.300/116.100	0.64	75	25	Tolbutamide: 269.1/170.0	0.77	-30	-8	Tolbutamide: 269.1/170.0	1.29	-100	-13
	Tolbutamide: 271.100/155.300	0.89	52	25								
MS Parameters	CUR (psi)	20			30				30			
	GS1 (psi)	50			60				55			
	GS2 (psi)	60			50				60			
	ion spray voltage (V)	5500			-4500				-4500			
	TEM (°C)	600			550				600			
	CAD	10			10				12			
	EP (eV)	10			-10				-10			
	CXP (eV)	15			-14				-12			

Quantitative analysis for X-05

Concentrations of X-05 in the samples were determined using calibration curve. The concentrations in samples were reported as nM with 3 decimal places and the figures listed for %Bias (and more generally all percentages) were rounded to 1 decimal place.

It was one set of calibration curve in each analytical run, which includes 8 none-zero standards. 7 none-zero standards were used for calibration curve. All of them were met the analytical acceptance criteria.

Two sets of QC samples consisting of low (one within 3x of the LLOQ), middle (one in the midrange) and high (75%-90% of the ULOQ) concentrations were included in the analysis. 5 QC samples met the analytical acceptance criteria.

Semi-quantitative analysis for control compounds

For control compounds nadolol, metoprolol, digoxin and E3S, no calibration curve and QC were applied during sample analysis. The peak area ratios of analyte/internal standard were used as compound concentration in samples.

Data analysis

The apparent permeability (P_{app}, cm/s), was calculated using the following equations:

$$P_{app} = \frac{V_R}{Area \times Time} \times \frac{[drug]_{receiver}}{[drug]_{initial,donor}} = \frac{V_R}{Area \times Time} \times \frac{C_R}{C_0}$$

Where V_R is the solution volume in the receiver chamber (0.075 mL on the apical side, 0.25 mL on the basolateral side); *Area* is the surface area for the insert membrane, i.e., 0.0804 cm^2 for the area of the monolayer; *Time* is incubation time, expressed in seconds, i.e., 7200 s (120 min) for the current experiment; C_0 is the initial concentration of test compound (nM) or peak area ratio (PAR) of control compounds in the donor chamber.

Results

Table S4: Permeability results for X-05

Conc. [a] (μM)	+ / - GF120918 (Conc. [a] 10μM)	A to B Receiver		B to A Receiver		T0 Sample		Papp (A to B) (× 10^{-6} cm/s)		Papp (B to A) (× 10^{-6} cm/s)	
		Measured Conc.[a]	DF[b]	Measured Conc.	DF[b]	Measured Conc.	DF[b]	Individual	Mean ± SD	Individual	Mean ± SD
2	-	2.579	1	41.494	3	530.320	3	0.70	0.63 ± 0.06	10.14	8.93 ± 1.05
	-	1.808		29.094		445.460		0.58		8.46	
	-	2.173		33.114		523.271		0.60		8.20	
	+	6.134		6.612		507.625		1.74	1.80 ± 0.05	1.69	1.51 ± 0.27
	+	6.107		6.199		487.837		1.80		1.65	
	+	6.277		4.549		489.251		1.85		1.20	
5	-	8.645		87.779		1260.438		0.99	0.81 ± 0.15	9.02	10.14 ± 1.20
	-	5.699		87.690		1137.673		0.72		9.99	
	-	5.564		98.270		1115.567		0.72		11.41	
	+	22.445		17.144		1170.609		2.76	2.11 ± 0.58	1.90	1.68 ± 0.46
	+	17.127		19.844		1285.747		1.92		2.00	
	+	13.761		10.686		1203.627		1.65		1.15	

a: Conc. means concentration.
b: DF means Dilution Factor.
SD means standard deviation.

Percent of Lucifer Yellow in basolateral well was calculated using the equation:

$$\%\ Lucifer\ \ Yellow\ = \frac{V_{Basolatera\ 1} \times RFU_{\ Basolatera\ 1}}{V_{Apical} \times RFU_{\ Apical} + V_{Basolatera\ 1} \times RFU_{\ Basolatera\ 1}} \times 100$$

where RFU_{Apical} and $RFU_{Basolateral}$ are the relative fluorescence unit values of Lucifer Yellow in the apical and basolateral wells, respectively; V_{Apical} and $V_{Basolateral}$ are the volume of apical and basolateral wells (0.075 and 0.25 mL), respectively.

Preparation of eight ASDs of X-05

X-05 and eight polymers (PVP K30, PVP VA 64, HPMCE5, HPMCAS-MG, Eudragit EPO, Eudragit L100, PEG 8000 and Soluplus) were prepared to ASDs at 10% drug loading on a Pilot

Table S5: Freeze drying cycle for ASDs

Procedure	Temperature (°C)	Duration Time (min)	Vacuum (Pa)
Freezing	-40	180	1
Primary drying	-10	300	50
	10	900	50
Secondary drying	30	30	50

1-2LD freeze dryer (Biocool, China), respectively. Briefly, 30 mg of X-05 and 270 mg of each polymer were dissolved in 6 mL of suitable solvent. The solvents used for Eudragit L100 were 1,4-dioxane/water (9:1, v/v); 1,4-dioxane/water (8:2, v/v) for HPMCAS-MG; 1,4-dioxane/water (1:1, v/v) for PVP K30; and 1,4-dioxane for the others. Pure X-05 dissolved in 1,4-dioxane as control. 2 mL of each solution was transferred into lyophilization vial and put into the freeze dryer. The freeze drying cycle and parameters were shown in table S1.

XRPD results

As shown in Figure S1, the disappearance of all typical sharp peaks of crystalline X-05 confirmed the amorphous nature of the ASDs following freeze drying in each polymer.

Kinetic solubility of X-05 and eight ASDs in FaSSIF

From Figure S2, the kinetic solubility showed that, all the seven ASDs could improve the solubility of X-05 in FaSSIF relative to X-05, except Eudragit EPO. Among which, PEG 8000 and

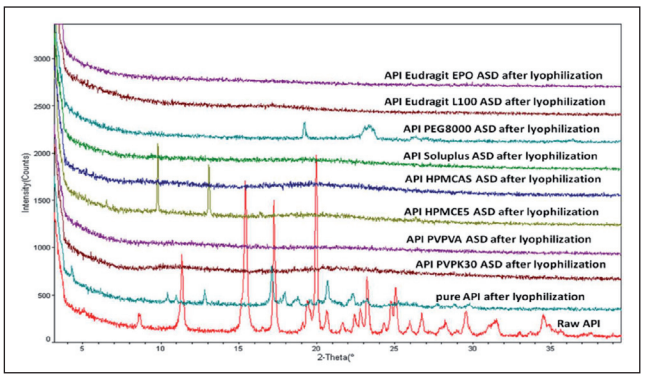

Fig. S1: XRPD patterns of eight ASDs (10% DL) and X-05.

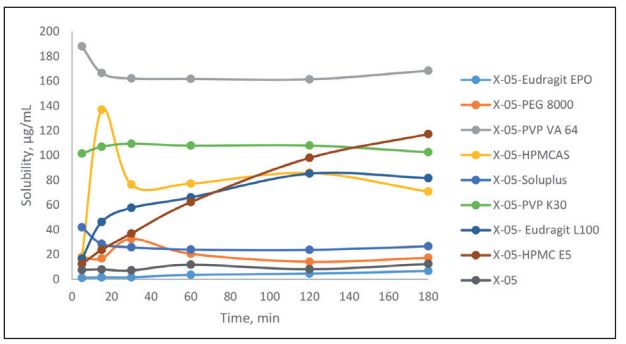

Fig. S2: Kinetic solubility profiles of ASDs (10% DL) and X-05 in FaSSIF at 37 °C.

Soluplus increased the solubility of X-05 as much as 3 folds, and the solubilization effect was weak. Even though the solubilisation effects of HPMC E5 and Eudragit L100 were stronger, their dissolution rate were slow. HPMCAS, PVP VA 64 and PVP K30 could increase the solubility of X-05 by more than 5, 13 and 8 times, respectively, and the solubilization effects were remarkable. Therefore, these three polymers were chosen to select the optimal carrier for X-05 to prepare amorphous solid.

Solid-state stability

ASD samples with PVP K30 (20% DL), PVP VA 64 (20% DL) and HPMCAS (20% DL) were exposed to 40 °C and 75% relative humidity (40 °C/75% RH) and 60 °C/ ambient RH for short-term stability studies. Detail results as show in Table S6 and Table S7.

Table S6: Stability study results of ASDs for up to 1 week (40 °C/75% RH)

Peak name	Peak Area, %					
	X-05-PVP K30		X-05-PVP VA 64		X-05-HPMCAS	
	Initial	1 week	Initial	1 week	Initial	1 week
X-05	99.62	99.58	99.65	99.65	99.49	99.35
RRT 0.95	--	0.07	--	--	0.14	0.21
RRT 0.98	--	--	--	--	--	0.09
RRT 1.04	0.38	0.35	0.35	0.35	0.37	0.35

Another stability studies of ASD samples with PVP VA 64 (30% DL, 40% DL and 50% DL) were performed for as long as 4 weeks at 40 °C/75% RH and 60 °C/ambient RH. Detail results as show in Table S8 and Table S9.

Table S7: Stability study results of ASDs for up to 1 week (60 °C/ambient RH)

Peak name	Peak Area, %					
	X-05-PVP K30		X-05-PVP VA 64		X-05-HPMCAS	
	Initial	1 week	Initial	1 week	Initial	1 week
X-05	99.62	99.45	99.65	99.65	99.49	99.11
RRT 0.95	--	0.19	--	--	0.14	0.23
RRT 0.98	--	--	--	--	--	0.30
RRT 1.04	0.38	0.36	0.35	0.35	0.37	0.36

Table S8: Stability study results of ASDs X-05-PVP VA 64 for up to 4 weeks (40 °C/75% RH)

Peak name	Peak area, %								
	30% DL			40% DL			50% DL		
	Initial	1 week	4 weeks	Initial	1 week	4 weeks	Initial	1 week	4 weeks
X-05	99.60	99.50	99.68	99.60	99.61	99.56	99.60	99.62	99.50
RRT 1.04	0.40	0.40	0.32	0.40	0.40	0.44	0.40	0.38	0.50

Table S9: Stability study results of ASDs X-05-PVP VA 64 for up to 4 weeks (60 °C/ambient RH)

Peak name	Peak Area, %								
	30% DL			40% DL			50% DL		
	Initial	1 week	4 weeks	Initial	1 week	4 weeks	Initial	1 week	4 weeks
X-05	99.60	99.61	99.66	99.60	99.60	99.55	99.60	99.60	99.48
RRT 1.04	0.40	0.39	0.34	0.40	0.40	0.45	0.40	0.40	0.52